Photon-echo nuclear double resonance and its application in ruby*

P. F. Liao, P. Hu,† R. Leigh,‡ and S. R. Hartmann
Columbia Radiation Laboratory, Department of Physics, Columbia University, New York, New York 10027
(Received 15 August 1973)

A photon-echo nuclear double resonance (PENDOR) experiment which detects nuclear magnetic resonances by monitoring the stimulated photon-echo intensity after the application of an rf pulse is described and used to determine the Cr-Al hyperfine and electric-quadrupole interaction parameters associated with the Cr^{3+} ion in the $^2E(\bar{E})$ optically excited state in ruby. Most of these parameters are found to be within a few percent of the values associated with Cr^{3+} in the $^4A_2$ ground state. Resonances are also observed associated with the latter state, and they are in agreement with previous spin-echo ENDOR work. High resolution is obtained by using a gated cw ruby laser which generates a rapid train of three-pulse stimulated-photon echoes with a long time interval between the second and third excitation pulses. The theoretical behavior of the PENDOR effect is discussed with emphasis on the ability to disentangle complicated multiple overlapping resonances by causing whole sets of resonances to disappear in a controlled way.

I. INTRODUCTION

Since its introduction in 1956 by Feher,[1] the technique of ENDOR (electron-nuclear double resonance) has proved to be an extremely important spectroscopic tool. This technique allows the precise measurement of the nuclear-magnetic-resonance spectra associated with nuclei lying near or at a paramagnetic center and provides a determination of the interactions between the nuclei and the center. The ENDOR method involves monitoring an electron spin resonance (ESR) microwave signal while simultaneously inducing nuclear transitions with an rf field. The nuclear resonances are indicated by a change in the ESR signal. Such data provide useful information concerning the spatial distribution of the electronic wave function and have contributed significantly to our present understanding of color centers in solids.[2] The ENDOR technique often can provide a tool in the determination of crystal structure, and applications for the determination of complex organic structures of biological significance remain to be fully exploited.

In a similar way, the knowledge of hyperfine and superhyperfine interactions between nuclei and an atom or ion in an optically excited state provides detailed information about the excited-state wave funtion and serves as a sensitive check of theoretical calculations. In gases, hyperfine interactions associated with excited states have been studied either by direct measurement of optical spectra[3] or with several optical-pumping techniques.[3,4] Naturally, the direct measurements are restricted to fairly strong hyperfine interactions. The use of ENDOR in the investigation of excited states in solids has been limited to a few materials which have large spin memory during an optical-pumping cycle; and, because only relatively small populations are produced in the excited state, the effect must be detected by optical means.[5]

Recently[6,7] an ENDOR technique involving the use of photon echoes[8] has been demonstrated in ruby. As the photon echo generally (not necessarily) involves an optical transition between the ground and excited states, nuclear resonances associated with the echo atom in both the ground and excited states, are usually observed. Because each nuclear resonance is detected optically, one obtains a great increase in signal-to-noise ratio. No Boltzmann population difference is required of the nuclear spin system. The great sensitivity of optical detection not only allows the observation of the extremely small excited-state population but also requires only a very small sample volume. (Typical volume excited in experiments to be described here is $\sim 10^{-5}$ cm^3.) The ability to detect resonances in such small volumes may prove to be very important in the study of organic molecules of biological interest, as many of these are quite difficult to grow.

The photon-echo nuclear double resonance (PENDOR) technique is the optical analog of spin-echo ENDOR[9-11] and consists of monitoring the three-pulse stimulated-photon-echo intensity[12] as a function of the frequency of a double resonance rf field applied to the sample in the time interval between the second and third excitation pulses (Fig. 1). If the rf field is resonant with a transition frequency of one of the nuclear neighbors, the resulting induced nuclear transition will alter the local field at the echo-atom site and hence will affect the coherent rephasing of the echo atom, leading to a reduction in echo intensity. Thus, by

measuring echo intensity as a function of the frequency of the rf field, we obtain spectra that reveal the precise energy of the nuclear transitions. From these energies one can deduce the electron-nuclear interaction parameters.

We have utilized the PENDOR technique in order to determine Cr-Al superhyperfine and electric quadrupole interaction parameters in ruby (Al_2O_3: Cr^{3+}) for the 14 nearest Al neighbors of a Cr^{3+} ion in the $^2E(\bar{E})$ excited state in ruby. Our work, which provides the major Cr-Al interaction constants to an accuracy of a few percent, confirms previous work,[13] which by an analysis of photon-echo relaxation and modulation behavior showed that the ground- and excited-state Cr-Al interaction parameters were of the same order of magnitude.

In Sec. II we discuss the theoretical behavior of the PENDOR effect using Ref. 11 as a basis. We stress the analysis whereby it is possible to disentangle complicated multiple overlapping resonances by causing whole sets of resonances to disappear in a controlled way. Section III details the experimental apparatus, while Sec. IV specifically pertains to the PENDOR technique as applied to ruby. We again stress the methods by which whole sets of lines can be manipulated and identified.

II. PENDOR

PENDOR is the optical analog of electron-spin-echo ENDOR, and hence the theoretical framework and discussion given in Refs. 9 and 11 describing spin-echo ENDOR remain valid. Rather than repeat the derivation of the echo ENDOR effect we shall simply restate the result and discuss its applicability to PENDOR.

The two states involved in the stimulated-photon-echo formation are connected via an electric dipole moment and are characterized by an optical frequency transition instead of a magnetic dipole moment and a microwave frequency transition, as is the case for electron spin echoes. In both cases, however, the energy separation between echo-atom states has a contribution from the interaction between the echo atom and nuclei, and this interaction allows the PENDOR effect. Therefore, just as in echo ENDOR, nuclear transitions which are induced by an externally applied rf field during the stimulated-echo-excitation-pulse sequence will be detected by a decrease in the stimulated-echo intensity.

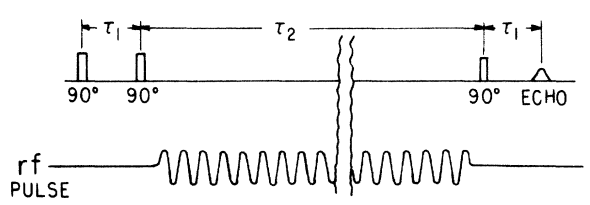

FIG. 1. PENDOR pulse sequence.

The stimulated-echo amplitude can be calculated with the following expression:

$$\langle \vec{P} \rangle = \mathrm{Tr}\vec{P}\rho, \tag{1}$$

where $\vec{P}$ is the dipole-moment operator. The quantity ρ is the density matrix at the time of the stimulated echo and is given by

$$\rho = e^{-(i/\hbar)H\tau_1} R_{90} U R_{90} e^{-(i/\hbar)H\tau_1} R_{90} \times \rho_0 R_{90}^{-1} e^{+(i/\hbar)H\tau_1} R_{90}^{-1} U R_{90}^{-1} e^{+(i/\hbar)H\tau_1}, \tag{2}$$

where ρ_0 is the density matrix before any excitation pulses are applied; R_{90} represents the time development due to a 90° excitation pulse; U represents the time development between the second and third 90° excitation pulses of the stimulated-echo-pulse sequence and includes the effect of the rf field on the nuclei.

The expression for the stimulated-echo amplitude, which is strictly valid only when the nuclear Hamiltonians commute, i.e., when $[h_1^k, h_2^k] = 0$, has been derived in Ref. 11 and is given as

$$\langle P_{\mathrm{STE}} \rangle = \tfrac{1}{4} C \left\{ 1 + \prod_k \left[1 - \frac{2}{2I_k + 1} \sin^2(\tfrac{1}{2}\theta) \times [1 - \cos(\omega_{lm}^{1k} - \omega_{lm}^{2k})\tau_1] \right] \right\}, \tag{3}$$

where

$$\omega_{lm}^{1k} = (1/\hbar)(E_{1l}^k - E_{1m}^k),$$

$$\omega_{lm}^{2k} = (1/\hbar)(E_{2l}^k - E_{2m}^k).$$

It is assumed that the kth nucleus has been double resonated with a θ-degree rf pulse and that the nuclear transition is between states labeled by l and m. The energy $E_{1\alpha}^k$ ($E_{2\alpha}^k$) is the eigenvalue of the nuclear Hamiltonian h_1^k (h_2^k) corresponding to the Hamiltonian of the kth nuclear neighbor in the neighborhood of the echo atom in the ground (excited) state 1 (2). C is a normalization factor. The ENDOR frequencies [corresponding to the ground (excited) state] of the nuclei labeled k are given by ω_{lm}^{1k} (ω_{lm}^{2k}). Generally, one observes photon-echo intensity rather than amplitude, in which case Eq. (3) should be squared. We find that, for ruby, $[h_1^k, h_2^k]$ is close enough to zero for Eq. (3) to be very useful.

According to Eq. (3), a significant decrease in stimulated-photon-echo intensity can be obtained whenever the rf pulse frequency equals that of

a nuclear transition. In the case of aluminum nuclei in ruby ($I=\frac{5}{2}$), a 180° rf pulse ($\theta=\pi$) acting on a neighboring nucleus produces a decrease in echo intensity of approximately 50% if τ_1 is chosen correctly. This decrease depends sinusoidally on τ_1, the time separation between the first two excitation pulses. This dependence on pulse separation arises because an induced nuclear transition produces a change $\Delta\omega=(\omega_{lm}^{1k}-\omega_{lm}^{2k})$ in the rephasing rate of the atomic dipoles and hence, when the stimulated echo is formed, the pseudomoment will have precessed an additional angle $\Delta\omega\tau_1$. The greatest PENDOR signal is obtained for $\Delta\omega\tau_1=(2n+1)\pi$ (integer n), in which case those echo atoms associated with resonated nuclei radiate out of phase with the other atoms and hence tend to cancel the echo. On the other hand, if $\Delta\omega\tau_1=2n\pi$, no PENDOR signal will result, as all atoms radiate in phase, and one observes a normal echo. This dependence on pulse separation provides a powerful tool for analyzing the observed spectra. For example, if, as in the case of ruby, the positions of the ground-state resonances are known, one can use the τ_1 dependence to calculate the positions of excited-state resonances. It is worth noting that in the case of spin-echo ENDOR, when (as again in the case of ruby) the major part of the electron-nuclear interaction is diagonal (i.e., $[h_1^k, h_2^k]\simeq 0$) and the interaction parameters are the same for both ground and excited states, the quantity $(\omega_{lm}^{1k}-\omega_{lm}^{2k})$ depends only weakly on m, and the $2I$ lines corresponding to the $2I$ nuclear transitions of a given nucleus all have essentially the same dependence on τ_1. As a result, one can almost immediately classify the $2I$ lines associated with a given nucleus together. For PENDOR, however, even when $[h_1^k, h_2^k]\simeq 0$, the inherent difference between the interaction constants in the two states can cause $(\omega_{lm}^{1k}-\omega_{lm}^{2k})$ to depend strongly on m. In this case the amplitudes of the PENDOR lines (i.e., the amplitude of the stimulated-echo degradation) of a nuclear set will not all have the same dependence on pulse separation, and we only retain the pairing of ground- and excited-state PENDOR lines. Fortunately, in ruby it is only the change in the nuclear quadrupole interaction which is important, and this change is small so that we are still able to group all lines of a given nuclear set together on this basis. When this grouping obtains, we can also considerably simplify the spectra by choosing τ_1 such that all lines associated with a given nuclear-neighbor site do not appear (see Figs. 5 and 6).

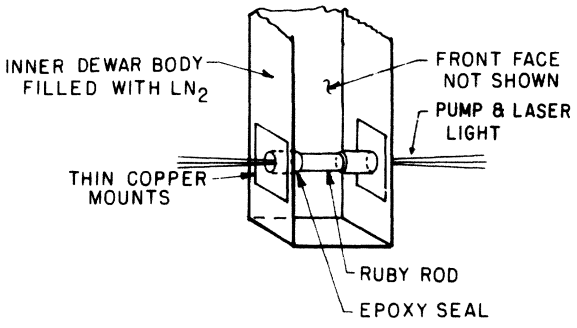

FIG. 2. Construction of cw ruby laser.

III. EXPERIMENTAL TECHNIQUE

The first PENDOR experiment[6] was performed with existing apparatus consisting of a nitrogen-cooled Q-switched ruby laser and two optical delay lines. Since the largest practical pulse delay obtainable was ~3 μsec, it was not possible to do more than demonstrate the general effect—the spectral resolution was too poor to permit observation of individual resonances.

In order to achieve high resolution we constructed a continuous ruby laser, whose output was gated by Pockels-cell light modulators to give the desired pulse sequences for photon-echo generation. With this apparatus we overcame the limitations on pulse delay and the associated problem of instability in the complex optical path. We have in fact seen stimulated echoes for pulse separation times as large as the 4-msec excited-state lifetime. Our laser, based on a design of Szabo,[14] consists of a 1.5-cm-long by 0.25-in.-diam cylinder of 0.05-wt% Czochrolski ruby, suspended in a bath of liquid nitrogen in the manner indicated in Fig. 2. Note that the pumping light and the laser light pass only through the antireflection-coated room-temperature windows and the uncoated ends of the rod.

The source of the pumping light is a Spectra Physics argon-ion laser with a nominal output of 1.5 W in the 5145-Å line which is focused into the rod by a 17-cm converging lens. Lasing at 6934 Å occurs in the cavity formed by the uncoated end faces of the rod with a threshold of a few hundred milliwatts of pump power and a maximum output (in the forward direction) of about 70 mW. [This apparatus has been improved and the pump power increased to 5 W. We now obtain 1 W at 6934 Å. See P. Liao and S. R. Hartmann, [Opt. Commun. 8, 310 (1973).] The data of Ref. 15 show that only the 5145-Å line of the argon laser is effective in pumping the rod and that the pumping is optimal when the vertical polarization of the pump light is perpendicular to the plane formed by the optic axis and the wave vector of the pump light. Therefore, the rod is mounted

with the optic axis, which is inclined 60° from the cylinder axis, in a horizontal plane. Lasing is optimal when the input face of the rod forms an additional cavity for the argon laser. The laser output is recollimated with a 13-cm lens, producing a parallel beam with a diffraction-limited divergence of ~0.8 mrad.

The entire apparatus is shown in Fig. 3. Filters remove the residual argon light from the ruby-laser beam, and a pair of Coherent Associates Pockels cells gate the beam on for the appropriate series of pulses. Each optical shutter consists of a pair of crossed Glan prism polarizers with a Pockels cell between them. When properly aligned and biased, the Pockels cell is completely passive, and the polarizers provide about 500:1 extinction, limited by crystal irregularities in the cell. When a pulse of 300 V is applied to the Pockels cell, it becomes a half-wave plate, rotating the polarization of light passing through it by 90°, thus negating the effect of the two polarizers. Thus, the two Pockels-cell gates, optically in series and electronically in parallel (to provide simultaneous opening), act as a fast shutter, each with an extinction ratio of about 500:1. Up to three high-voltage pulses are provided by a homemade circuit which discharges coaxial cables through EG&G Krytons. A set of electronic pulsers provides timing flexibility for the system.

After gating, the beam is expanded and focused down to a spot of 5×10^{-3}-cm calculated diameter on the ruby sample by a pair of converging lenses acting as a telescope. With this configuration

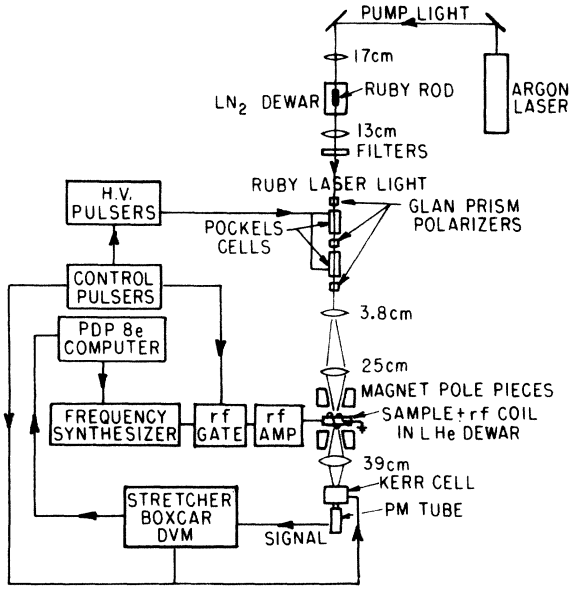

FIG. 3. Schematic diagram of experimental setup.

the laser power necessary to produce a 100-nsec 90° pulse is only a few milliwatts. The alignment of the Pockels cells and the telescoping lenses is quite critical, and these are each provided with gimbelled angular adjustment mounts and a pair of orthogonal micrometer-driven translators. Almost all transmitting optical components are antireflection coated to provide maximum power into the sample. The quarter-wave plates allow transition selection, and the sample is mounted in a Janis Super VariTemp helium Dewar and maintained at 3°K or below to minimize spin-lattice relaxation during the intervals between pulses. The echo is detected by a photomultiplier, which is protected from the laser pulses by a Kerr cell which is pulsed open shortly before the echo is expected.

The rf field for resonating the Al nuclei is supplied by a pair of 1.3 μH coils wound around the sample, which consists of a $3.0\times10\times2.5$-mm segment of 0.005-wt% ruby. The coils are energized by a broadband 3-W amplifier driven by a Hewlett-Packard frequency synthesizer whose output is gated on between the second and third laser pulses. The frequency of the synthesizer is controlled by a PDP-8e computer through an interface constructed here.

The dc magnetic field is supplied by a Varian current-regulated magnet with 4-in. iron pole pieces, axially bored to permit the passage of the excitation pulses. The consistency of the results to be reported below indicates that the field, once set, is stable to better than 0.05%. The field is set initially using a Bell Hall probe gaussmeter, whose probe is attached to the outside of the Dewar near the sample. This is calibrated to read the field at the point on the sample where echoes are produced by finding the dip in echo amplitude at the 2.06-kG ground-state level crossing of ruby. Finer calibration from resonance lines indicates that this method is accurate to 0.05%.

As in previous experiments,[6,7] the echo pulse from the photomultiplier is fed into a gated stretcher, which produces a fast-rising pulse whose amplitude is proportional to the integral of the echo pulse and has a decay of 3 μsec. The resulting series of pulses is fed into a boxcar averager, the output of which is at a level equivalent to a weighted average of recent input pulses, where the weight of a particular input pulse is an exponentially decaying function of time. The time constant of the device is set so that the $1/e$ decay time corresponds to about 10 pulses.

After every tenth echo, the computer resets the rf frequency, reads the boxcar through a digital volt meter, and adds the values obtained

to a channel corresponding to the preceding frequency. Usually, each channel corresponds to 2 kHz, and the computer drives the frequency synthesizer through a sweep covering 1 MHz, thus using 500 channels. Most data are the result of 16 such sweeps, and so each point represents an average of 160 echoes. The entire apparatus can produce about 30 echoes per second, limited by the repetition rate of the Kerr cell that protects the photomultiplier. In addition, the computer can plot out the current or final results on an X-Y plotter or display them on an oscilloscope. A permanent record of each run is also punched out on eight-track paper tape.

IV. PENDOR IN RUBY

The $^4A_2$ ground state of the Cr^{3+} ion in ruby is an orbital singlet with a fourfold spin degeneracy, split into two Kramers doublets with spins $\pm\frac{3}{2}$ and $\pm\frac{1}{2}$, respectively, by the combined effect of the spin-orbit perturbation and the trigonal part of the crystal field. The first excited state of the Cr^{3+} ion is labeled $^2E(\bar{E})$ and is again a Kramers doublet with spin $\pm\frac{1}{2}$. These energy levels and the two independent circularly polarized transitions with which we obtained photon echoes are shown in Fig. 4.

Each Cr^{3+} ion in ruby is surrounded by an array of Al ions having nuclear spin $I=\frac{5}{2}$, and the interaction of the Cr electronic spin with the nearest of these nuclear spins is the subject of this investigation. The nearest-neighboring Al nuclear sites are listed in Table I, showing their coordinates relative to an origin at the Cr^{3+} site, with

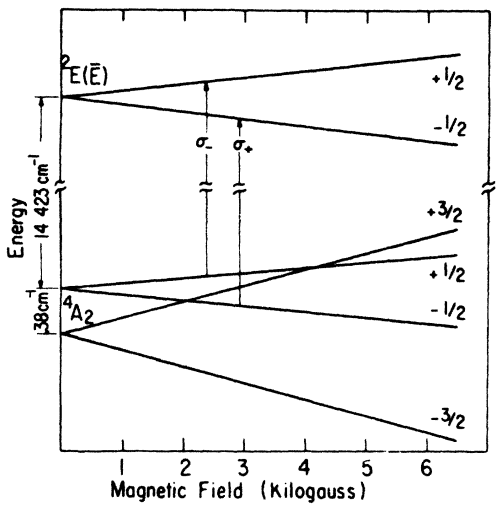

FIG. 4. Energy levels of ruby R_1 line for magnetic field applied parallel to c axis. σ_- and σ_+ denote the two independent circularly polarized transitions used in photon-echo generation.

the $\hat{z}$ axis along the crystalline optic axis. Following the notation of Ref. 16, a letter denotes each nuclear set, where all the nuclei in a given set have the same $\hat{z}$ coordinate and are symmetrically distributed in the $\hat{x}$-$\hat{y}$ plane. Thus they have equivalent magnetic interactions with the Cr^{3+} spin when the applied magnetic field is along the $\hat{z}$ axis, and the constants characterizing the interactions are the same within a set. For later reference, we include in Table I the magnetic fields at the nuclear sites which would be produced by a point dipole equivalent to the electronic spin situated at the Cr^{3+} site. The interactions between the nearby nuclei and the Cr^{3+} ion in the $^4A_2$ ground state have been studied both with standard ENDOR techniques[14] and with spin-echo ENDOR.[10,11] The more recent echo ENDOR experiments[10,11] have shown that the following interaction Hamiltonian can explain the observed echo ENDOR spectra when the magnetic field is applied parallel to the optic axis:

$$h^j = -\hbar\gamma H I_z^j + S_z[(A+B_z)^j I_z^j + B_t^j I_\alpha^j] + Q^j e^{-i\theta_1 I_\beta^j} e^{-i\theta_2 I_\alpha^j} e^{-i\theta_3 I_z} \times [I_z^{j\,2} + (\eta/3)(I_\alpha^{j\,2} - I_\beta^{j\,2})]\, e^{i\theta_3 I_z^j}\, e^{i\theta_2 I_\alpha^j} e^{i\theta_1 I_\beta^j}. \quad (3)$$

The subscripts α, β refer to directions in the transverse plane parallel to and perpendicular to the transverse component of the local field at the aluminum neighbor site, respectively. This Hamiltonian corresponds to either h_1^j or h_2^j if the interaction constants corresponding to states 1 or 2, respectively, are used. The first term in h^j represents the Zeeman interaction of the nuclear spin I with the external field. The second

TABLE I. Coordinates of the 14 nearest Al neighbors of the Cr^{3+} ion in ruby and the point dipole Cr-Al interaction constants for $^2E(\bar{E})$ state.

Neighbor set	G	I	J	K	L	N
(B_z) point dipole (MHz)	2.48	−1.01	0.09	−0.18	0.09	0.94
(B_t) point dipole (MHz)	0.0	0.68	0.86	1.02	0.86	0.0
Coordinates of nuclear neighbors [a]	0.0	0.27	0.54	0.54	0.27	0.0
	0.0	0.46	0.0	0.0	0.46	0.0
	−0.53	−0.11	−0.42	0.31	0.42	0.72
		0.27	−0.27	−0.27	0.27	
		−0.46	0.46	0.46	−0.46	
		−0.11	−0.42	0.31	0.42	
		−0.54	−0.27	−0.27	−0.54	
		0.0	−0.46	−0.46	0.0	
		−0.11	−0.42	0.31	0.42	

[a] Coordinates given in terms of rhombohedral cell dimension $a_0 = 5.137$ Å with Cr^{3+} at origin.

represents the effective magnetic field of the Cr^{3+} spin S_z at the nuclear site, dotted into the nuclear spin vector. The effective field contains contributions from both a dipole-dipole interaction, represented by parameters B_z and B_t, and from the contact interaction, given by parameter A, which measures the density of the Cr electron cloud at the nuclear site as transferred through the orbitals of the oxygen and aluminum electron clouds. The parameter Q gives the strength of the electric quadrupole interaction, while θ_1, θ_2, and θ_3 describe a tilt of the principal axis of the electric field gradient away from the optic axis, and η allows for an asymmetric field gradient. This Hamiltonain has proven adequate to explain the observed PENDOR spectra which we have associated with the $^2E(\bar{E})$ excited state.

Given a set of parameters, the Hamiltonian may be diagonalized numerically, but it is more convenient, especially for purposes of fitting the parameters, to use the following second-order perturbation expansion. The frequency of a nuclear spin transition from the mth to the $(m+1)$st level can be expressed as[10]

$$\omega_{m,m+1} = \omega_c - P''' + (m+\tfrac{1}{2})P' + (m+\tfrac{1}{2})^2 P'', \qquad (4)$$

where

$$P' = Q\{3\cos^2\theta_2\cos^2\Phi - 1 + \eta \times[\cos 2\theta_3(\sin^2\Phi - \cos^2\Phi\sin^2\theta_2) - \sin 2\theta_3 \sin\theta_2 \sin 2\Phi]\},$$

$$P'' = (Q^2/3\omega_c)[36(\Phi^2 + \theta_2^2) - \eta^2],$$

$$P''' = (8Q^2/9\omega_c)[18(\Phi^2 + \theta_2^2) - \eta^2],$$

$$\omega_c = (\gamma/2\pi)|H_{\text{eff}}|,$$

$$\Phi = \theta_1 - \theta,$$

$$\tan\theta = B_t S_z/[(A+B_z)S_z - (\gamma/2\pi)H],$$

$$\vec{H}_{\text{eff}} = \{[(A+B_z)S_z - (\gamma/2\pi)H]\hat{z} + B_t S_z \hat{e}_\alpha\}(2\pi/\gamma),$$

and where P'' and P''' are of second order in η, θ_1, and θ_2.

The ENDOR frequencies are given by $\omega_{m,m+1}$, while the change in the rephasing rate caused by inducing a nuclear transition is

$$\Delta\omega = (\omega_c^1 - \omega_c^2) - (P_1''' - P_2''') + (m+\tfrac{1}{2})(P_1' - P_2') + (m+\tfrac{1}{2})^2(P_1'' - P_2''),$$

where the label 1 (2) refers to the ground- (excited-) echo-atom-state parameter. If $[h_1^k, h_2^k] = 0$, then θ in Eq. (4) is zero, and hence $P_1' = P_2'$, $P_1'' = P_2''$, and $P_1''' = P_2'''$ when the interaction parameters are independent of the echo-atom states, as obtained in ordinary echo ENDOR. For ruby, where $I = \frac{5}{2}$ and the large contact interaction[16] allows setting $[h_1^k, h_2^k] \simeq 0$ (those more-remote Al nuclei whose contact interaction is small also interact more weakly through the dipolar interaction, which is then small compared to the nuclear Zeeman interaction), $\Delta\omega$ then has essentially the same value for all ten nuclear transitions for a particular nucleus associated with a ground-state or excited-state echo atom. In the case of PENDOR, however, the associated P', P'', and P''' depend on the echo-atom state, so strictly speaking there are only two nuclear transitions associated with each value of $\Delta\omega$. However, as indicated earlier, as a practical matter we find that the difference of P', P'', and P''' between their value in the two echo-atom states is sufficiently small [owing to the small change in the interaction parameters associated with the $\bar{E}(^2E)$ excited state as compared to those in the $^4A_2$ ground state] so that $\Delta\omega$ is effectively independent of m.

To obtain the excited-state interaction parameters in ruby, PENDOR spectra were measured at magnetic fields of 1, 2, 3, and 5 kG. Several representative spectra are shown in Figs. 5–7. The experiments covered both σ_+ and σ_- transitions for the entire range of radiofrequencies where resonances were expected, except for a few cases involving the σ_- transition. (In these cases the effective field of the Cr^{3+} ion almost cancels an external field of 1 or 2 kG, driving the resonance frequencies down into the kHz range and below the range of our rf amplifier.)

The spectra show dips in echo intensity, on resonance, going down to about 50% of the off-resonance case and having a full width as narrow as 25 kHz. The source of this width is primarily

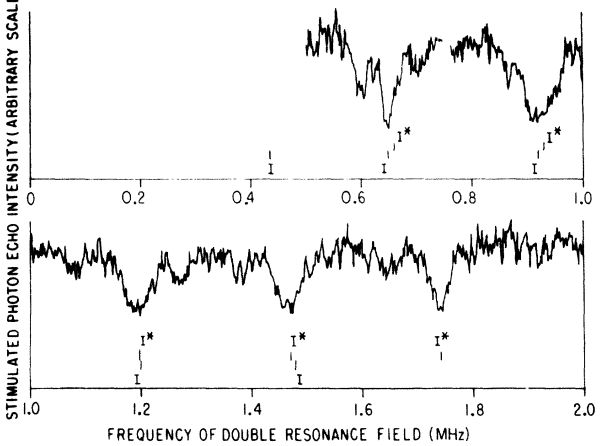

FIG. 5. PENDOR spectra at 1.9 kG for σ_- transition. $\tau_1 = 1.5$ μsec; $\tau_2 = 50$ μsec. Note only resonances due to nuclear neighbor type I give substantial PENDOR signals.

the Fourier broadening of a typical 50-μsec rf pulse, about 20 kHz. A small contribution to the observed width may come from the 2-kHz width of the data channels, which could possibly be doubled to 4 kHz by the approximations of the electronic averaging in the boxcar unit.

It should be noted that resonance lines corresponding to the $^4A_2(+\frac{1}{2})$ ground-state sublevel have not appeared in our spectra. The reasons for this are unclear at present, but the presence of a shallow-dip stretching across the relevant spectra may indicate that these lines may have broadened beyond recognition. The shallow dip may have resulted from a long-term drift; however, similar behavior has been found in the electron-spin-echo ENDOR spectra[11] for the $^4A_2$ ground state. In that case echo ENDOR resonances associated with the $+\frac{1}{2}$ magnetic sublevel were found to be broad at 5.8 kG, and at 3.3 kG were too broad to be detected.

The nuclear set responsible for a given PENDOR line in Figs. 5–7 is indicated by a letter below the line in the spectra. Resonances associated with the excited state are denoted by an asterisk. The identification of these lines involved several stages. First, the interaction constants corresponding with the ground state had been determined by electron-spin-echo ENDOR experiments, and the idenficitation of the corresponding PENDOR lines was easily made. All of the observed PENDOR lines which we associated with the ground state are in good agreement with the results of Ref. 11. The remaining lines were then identified on the basis of similarity to the ground-state resonances. In particular, the separation between each of the $2I$ resonance lines of a given nuclear set is equal to approximately $2Q$, and this separation is not expected to differ much from the ground-state value. Also of major importance was the dependence of the echo ENDOR effect on the pulse separation τ_1. As an example, we note that one set of six lines always appeared first as the pulse separation τ_1 was increased (Fig. 5). Five of these lines corresponded to the expected ground-state resonances of nuclear-neighbor set I. Recalling the dependence of PENDOR spectra on the product of τ_1 and the difference between nuclear resonance frequencies corresponding to the ground and excited states, we increased τ_1 so that $\Delta\omega\tau_1 = 2\pi$, where $\Delta\omega$ is the (approximately equal) separation of these six lines. Other lines then appeared; however, the

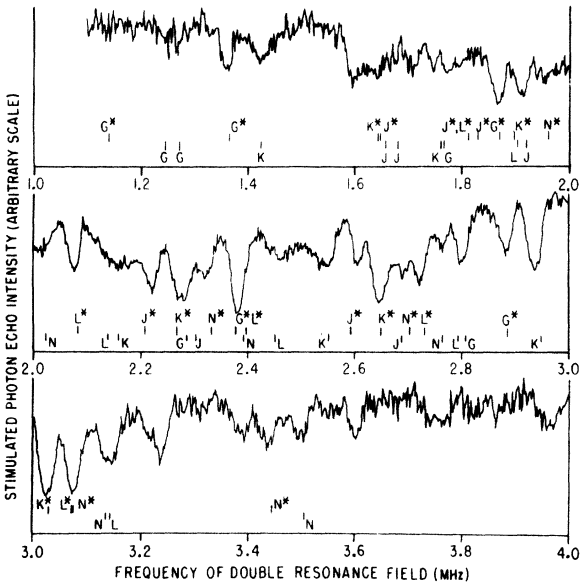

FIG. 6. PENDOR spectra at 1.9 kG for σ_- transition. $\tau_1 = 3.4$ μsec; $\tau_2 = 50$ μsec. Note resonances due to nuclear neighbor type I do not appear.

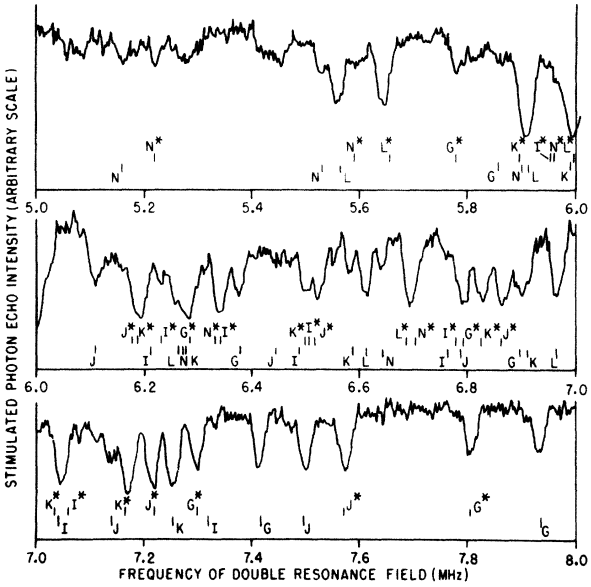

FIG. 7. PENDOR spectra at 5.0 kG for σ_+ transition. $\tau_1 = 3.9$ μsec; $\tau_2 = 50$ μsec.

TABLE II. Cr-Al interaction constants in ruby for Cr^{3+} in $^2E(\bar{E})$ excited state.

Nuclear set	G	I	J	K	L	N
$A + B_z \pm 0.01$ (MHz)	2.485	1.901	2.597	1.878	1.554	0.822
$B_t \pm 0.05$ (MHz)	0.0	0.538	0.993	1.035	0.865	0.0
$2Q \pm 0.01$ (MHz)	0.506	0.282	0.378	0.384	0.358	0.364
$\theta_1 \pm 0.1$ (rad)	0.0	−0.008	−0.10	−0.240	−0.070	0.0
$\theta_2 \pm 0.3$ (rad)	0.0	−0.02	0.140	0.070	−0.070	0.0
$\theta_3 \pm 0.5$ (rad)	0.0	0.58	0.130	0.100	0.670	0.0
$\eta \pm 0.5$	0.0	0.82	−0.430	−0.390	0.740	0.0
$A_{(2)}$ (MHz)	0.005	2.91	2.51	2.06	1.46	−0.12
$A_{(2)}/A_{(1)}$	0.007	0.90	1.06	0.93	1.11	2.0

original six disappeared. This dependence on pulse separation indicated that the original six lines were in fact composed of the five ground-state and five excited-state resonance lines of nuclear neighbor set I. The interaction parameters for the excited state differed from those of the ground state by just enough to shift the lines by an amount equal to their separation. As noted previously, the ability to choose a pulse separation at which neighbor-set-I resonances do not appear also allows us to simplify considerably the spectra's appearance.

In Figs. 6 and 7 additional resonance lines which are not due to the nearest ten Al neighbors are visible. These lines are resonances of more distant nuclei. Because of insufficient signal-to-noise ratio we were not able to identify positively these lines and hence have left them unlabeled.

Precise knowledge of the interaction constants clearly depends on precise knowledge of the applied magnetic field. This problem was overcome by deducing the field from the positions of the lines corresponding to the ground-state resonances of neighbors G and N, as the ground-state interaction constants are known. In this way the excited-state interaction parameters for neighbors G and N were determined, and with these parameters the external field could be determined for those data sets on which the ground lines did not appear. The values of the external field H determined in this manner were thought to be accurate to about 0.1%.

In Table II we tabulate the excited-state Cr-Al hyperfine and electric quadrupole parameters which were determined from a least-squares fit to all of our PENDOR spectra. The least-squares fitting procedure utilized the perturbation expansion of the PENDOR frequencies and was performed on a PDP-8e minicomputer. The use of the minicomputer allows one to interact directly with the fitting procedure, a factor of utmost importance when fitting a function of many variables. The lines drawn below the spectra in Figs. 5–7 indicate the theoretical resonance frequencies obtained by a numerical determination of the eigenvalues of Eq. (3). This calculation was performed on an IBM 360 computer and utilized the parameters given in Table II and in Ref. 11. The fit shown here is typical of the fit to all our data.

The results of the fit are quite interesting. For the most part the excited-state parameters do not differ significantly from the corresponding ground-state values, with one notable exception. The parameters B_g and B_t are generally taken to represent the magnetic dipole-dipole interaction between the Cr^{3+} ion and the Al nucleus, while the parameter A gives the isotropic Fermi contact interaction. For the excited state, the values of B_t(i.e., $B_{t(2)}$) listed in Table II are in fair agreement with the point dipole-dipole approximation tabulated in Table I. Therefore, as a first approximation, one can use the point dipole-dipole values to estimate the excited-state contact interaction. The values of $A_{(2)}$ given in Table II were determined in this manner. The parameters $A_{(2)}$ and $B_{g(2)}$ could not be determined separately since photon echoes in ruby can only be observed for one orientation of the magnetic field (H parallel to the crystalline optic axis). Also listed in Table II are the ratios of the estimated values of $A_{(2)}$ to the estimated ground-state value $A_{(1)}$. As previously anticipated, this ratio is approximately 1.0 for all but G and N nuclei. The excited-state exchange interaction of nuclear neighbor G is essentially equal to zero. This neighbor is the nearest neighbor and lies directly above the Cr^{3+} ion on the optic axis. (This ratio may have limited meaning for nuclear neighbor N, since both $A_{(1)}$ and $A_{(2)} \sim 0$.) The rather striking behavior which we have observed may serve as an excellent test of a molecular orbital calculation of the exchange parameters.

Knowledge of the parameters allows one to calculate a lower limit for the linewidth of the optical transition $^2E(\bar{E}) \rightarrow {}^4A_2$. Using a method similar to that which has been applied to the computation of the electron-spin-resonance linewidth in ruby,[17] we obtain broadening of the optical transition of 0.54 MHz for the $^2E(\bar{E})(\pm\frac{1}{2}) \rightarrow {}^4A_2(\pm\frac{1}{2})$ transition and 8.9 MHz for the $^2E(\bar{E})(\pm\frac{1}{2}) \rightarrow {}^4A_2(\pm\frac{3}{2})$ transition. These linewidths represent the contribution to the optical linewidth produced by the Cr-Al interaction.

In conclusion, we have demonstrated a powerful technique for the probing of magnetic interactions of optically excited ions by the use of photon echoes. The echoes were generated with a technique utilizing a cw laser of relatively low power. With the availability of tunable dye lasers, these techniques will permit the study of a wide range of materials.

*This work was supported in part by the Joint Services Electronics Program (U. S. Army, U. S. Navy, and U. S. Air Force) under Contract No. DAAB07-69-C-0383, and in part by the National Science Foundation under Grant No. NSF-GH-38503x.

†Present address: Bell Telephone Laboratories, Murray Hill, New Jersey 07974.

‡Present address: Department of Physics, The City College of the CUNY, New York, New York 10031.

[1]G. Feher, Phys. Rev. 103, 834 (1956); 114, 1219 (1959).

[2]G. Feher, Phys. Rev. 105, 1122 (1957); R. Gazzinelli and R. Mieher, Phys. Rev. Lett. 12, 644 (1964).

[3]H. Koppermann, *Pure and Applied Physics*, Vol. 2 of *Nuclear Moments*, English version prepared by E. E. Schneider (Academic, New York, 1958), p. 82.

[4]F. D. Colegrove, P. A. Franken, R. R. Lewis, and R. H. Sands, Phys. Rev. Lett. 3, 420 (1959); P. A. Franken, Phys. Rev. 121, 508 (1961); M. E. Rose and R. L. Carovillano, Phys. Rev. 122, 1185 (1961); A. Kastler and J. Brossel, C. R. Acad. Sci. (Paris) 229, 1213 (1949); J. Brossel and F. Bitter, Phys. Rev. 86, 308 (1952).

[5]L. F. Mollenauer and S. Pan, Phys. Rev. B 6, 772 (1972).

[6]P. Hu, R. Leigh, and S. R. Hartmann, Phys. Lett. A 40, 164 (1972).

[7]P. F. Liao, R. Leigh, P. Hu, and S. R. Hartmann, Phys. Lett. A 41, 285 (1972).

[8]I. D. Abella, N. A. Kurnit, and S. R. Hartmann, Phys. Rev. 141, 391 (1966).

[9]W. B. Mims, Proc. R. Soc. Lond. 283, 452 (1965).

[10]P. F. Liao and S. R. Hartmann, Phys. Lett. A 38, 295 (1972).

[11]P. F. Liao and S. R. Hartmann, Phys. Rev. B 8, 69 (1973).

[12]N. A. Kurnit and S. R. Hartmann, *Interaction of Radiation with Solids* (Plenum, New York, 1967), pp. 693–701.

[13]D. Grischkowsky and S. R. Hartmann, Phys. Rev. B 2, 60 (1970); L. Q. Lambert, Phys. Rev. B 7, 1834 (1973).

[14]A. Szabo, Phys. Rev. Lett. 27, 323 (1971).

[15]T. H. Maiman, R. H. Hoskins, I. J. D'Haenens, C. K. Asawa, and V. Evtuhov, Phys. Rev. 123, 1151 (1961).

[16]N. Laurance, E. C. McIrvine, and J. Lambe, J. Phys. Chem. Solids 23, 515 (1962).

[17]R. F. Wenzel, Phys. Rev. B 1, 3109 (1970).